Self-organization with traveling waves: A case for a convective torus

Bice S. Martincigh
Department of Chemistry and Applied Chemistry, University of Natal, Private Bag X10, Dalbridge 4014, Republic of South Africa

Cordelia R. Chinake
Department of Chemistry, University of Natal, Private Bag X01, Scottsville 3209, Republic of South Africa

Tony Howes
Department of Chemical Engineering, University of Queensland, St. Lucia 4072, Brisbane, Australia

Reuben H. Simoyi*
Chemistry Department, West Virginia University, Morgantown, West Virginia 26506-6045
(Received 20 January 1997)

A traveling wave of $BaSO_4$ in the chlorite-thiourea reaction has shown concentric precipitation patterns upon being triggered by the autocatalyst HOCl. The precipitation patterns show circular rings of alternate null and full precipitation regions. This self-organization appears to be the result of the formation of a convective torus. The formation of the convective torus can be described as a Bénard-Marangoni instability with lateral heating. [S1063-651X(97)14406-3]

PACS number(s): 47.20.Dr, 47.70.Fw, 82.20.Mj

INTRODUCTION

Symmetry-breaking bifurcations in excitable chemical media can now be easily justified as due to a coupling of nonlinear kinetics and diffusion [1]. A typical case of local activation with lateral inhibition [2] would involve a scenario in which faster-diffusing components of the reaction inhibited the reaction while slower, low diffusivity components catalyzed the reaction system. If the diffusivities differ sufficiently enough, time-independent spatial inhomogeneities can be generated. Such patterning of an intrinsic length scale has been studied extensively, as it can lead to a mathematical and chemical rationalization of the phenomenon of morphogenesis [3].

Isothermal reaction-diffusion systems without convection can be replicated in gels [4], but are impossible to maintain in a more realistic aqueous chemical environment [5]. It has now been established that convection is a major driving force in chemically driven lateral instabilities [6]. We are just beginning to unravel the wide range of nonlinear dynamical behavior which is generated when convection is not suppressed [7]. In this paper we report on the fascinating dynamical behavior and self-organization that is observed in the symmetry-breaking bifurcations of an autocatalytic, highly exothermic chemical reaction system.

The chemical reaction system involved is part of a general set that involves the oxidation of a sulfur center in small organic molecules to sulfate, SO_4^{2-}, by a suitable oxyhalogen species such as bromate BrO_3^-, iodate IO_3^-, and chlorite ClO_2^- [8]. The data reported here are from the reaction of chlorite with thiourea [9]:

$$2ClO_2^- + SC(NH_2)_2 + H_2O \rightarrow 2Cl^- + SO_4^{2-} + OC(NH_2)_2 + 2H^+. \quad (A)$$

Reaction (A) is controlled by quadratic autocatalysis in hypochlorous acid, HOCl [10,11]. A traveling wave of SO_4^{2-} or acid can be initiated by addition of a drop of a weak solution of HOCl or allowed to generate spontaneously.

The progress of reaction (A) can be followed by several indicators, but the one chosen for this study is $BaSO_4$ precipitation. By spiking the solution with 0.048 M $BaCl_2$, any SO_4^{2-} formation will immediately be detected by the appearance of white $BaSO_4$ crystals. The irregular nature of the $BaSO_4$ precipitate particles allow us not only to determine the position of the wave front, but also the magnitude and direction of hydrodynamic activity at both in front of as well as behind the wave front. $BaSO_4$ precipitation patterns can be an effective instantaneous ''fingerprint'' of fluid motion in the wake of the wave front.

Such ''fingerprinting'' is very important because convective instabilities will ultimately destroy any emerging patterns. Thus any patterns obtained will be transient, but can be ''frozen'' a little longer by the use of $BaSO_4$. $BaSO_4$ crystals, which have a specific gravity of 4.500, will eventually sediment.

The property that sets these chemical systems apart from other pattern-generating chemical systems is the large evolution of heat at the wave front. In our controlled experiments the temperature gradient was maintained at $\Delta T = 3.8$ °C, although much higher jumps of over 70 °C could be produced by altering initial reactant concentrations. Our previous studies established the Marangoni effect as the most effective force contributing to lateral wave velocities [7]. By allowing the chemical system to control the temperature (no thermostating), and allowing convection to be established (aqueous, nongelled environments), very interesting, hitherto unob-

*Author to whom correspondence should be addressed.

served complex dynamical behavior has been reported. Among these are volcanic-type thermal plumes [12] as well as fingering patterns [13].

An important question to ask is whether any other combination of forces apart from reaction-diffusion can give rise to stationary Turing-type solutions? The Rayleigh-Bénard convection and Taylor-vortex flow are two dissipative dynamical systems which seem to be heavily dependent on the geometry of the experimental setup [14]. Boundary effects have also been very important in our chemical system, as the generation of the big wave is intrinsically different depending upon the size and geometry of the reaction vessel [7]. The experiments reported in this paper were observed in two large plexiglass vessels, large enough so as to minimize boundary effects (and assume an unbounded x-y plane). One was a rectangle of length 24.3 cm and width 15.3 cm, and the other an isosceles triangle of base 16.0 cm and a peak angle of 38°.

Although the reagent solutions were not thermostated, the starting temperature was maintained at 22.5 ± 1.0 °C. The important dynamical and bifurcation parameter was ΔT, the temperature jump at the wave front. The temperature was monitored by using a series of digital thermometers equipped with ultrafast response naked-bead type-K thermocouples. These thermocouples were lined up along the line of wave propagation, and correlations could be drawn between ΔT and the position of the wave front. The reagent solutions (2.0×10^{-2} M thiourea, 4.0×10^{-2} M chlorite, and 0.0488 M barium chloride) were vigorously mixed in a beaker, poured into the reaction vessel, and allowed to settle for 60 s (to allow physical ripples to disappear) before being triggered by a drop of a dilute solution of the autocatalyst HOCl. Experimental observations were done by means of a standard CCD Pulnix TMC 74 color camera attached to a Sony PVM-1334Q RGB monitor and a Panasonic AG-1960 professional video recorder. Desired frames were captured using a PCVision Plus frame grabber and stored as 640×480 square-pixel images. Image analysis and filtering was via Bioscan Optimas software.

RESULTS

The most important parameter apart from ΔT was the depth of the solution. For the exotic dynamics reported here the depth d was in the range $1.7\leqslant d\leqslant3.3$ mm.

Bifurcation sequence: The wave velocity initially accelerates to some high velocity, and then decelerates to attain a constant lateral velocity. During the initial acceleration the reaction solution produces a series of distinct concentric precipitation patterns, where one observes alternating rings of $BaSO_4$ precipitation and null precipitation. This patterning is short-lived, lasts about 5 s, and can, within that period, form 3–7 such concentric rings. Figure 1 shows experimental data of four such rings in a typical experiment. This type of patterning ceases when the wave velocity increases past some threshold value which is determined by a complex interaction between ΔT, initial concentrations, solution viscosity, depth of solution, and vessel geometry.

At the end of the concentric patterning, there is an abrupt change in hydrodynamic activity, and the precipitation patterns begin to show longitudinal alignment in the direction of wave propagation (concentric patterns are distinctly perpendicular to the direction of wave propagation). Figure 2 shows longitudinal patterns after the concentric patterns had been formed. Due to the violent hydrodynamic activity, the concentric patterns by this time will be slightly distorted. The longitudinal patterns are observed during the period when the wave velocity attains its maximum value.

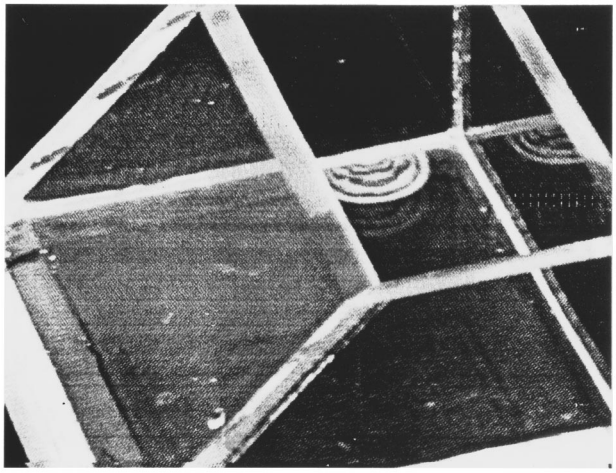

FIG. 1. Image of the concentric circles formed from a reaction solution triggered from the edge of the reaction vessel. Four distinct circular bands of precipitation can be seen. $[ClO_2^-]_0=2.25\times10^{-2}$ M, $[SC(NH_2)_2]_0=1.13\times10^{-2}$ M, and $[BaCl_2]_0=0.048$ M.

The wave finally decelerates to attain a constant steady velocity until it reaches the edge of the container. In an unbounded plane, this wave velocity can be maintained indefinitely. In this region, the wave produces thermal plumes once every 7–10 s in a region behind an area of faint precipitation. The thermal plumes have been reported elsewhere [12]. Normally, by the time the plumes and faint precipitation regions appear, patterning in the concentric patterns region would have been annihilated. Figure 2 shows the slightly distorted convective tori by the time the longitudinal

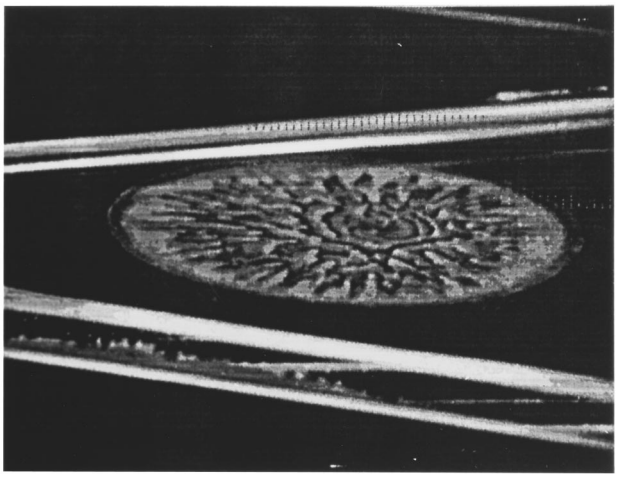

FIG. 2. Picture of the progress of a wave initiated in the center of the vessel. The inner part of the wave has circular patterning which bifurcates to longitudinal patterning as the wave velocity increases. $[ClO_2^-]_0=4.5\times10^{-2}$ M, $[SC(NH_2)_2]_0=2.3\times10^{-2}$ M, $[BaCl_2]_0=0.03$ M, and $d=1.7$ mm.

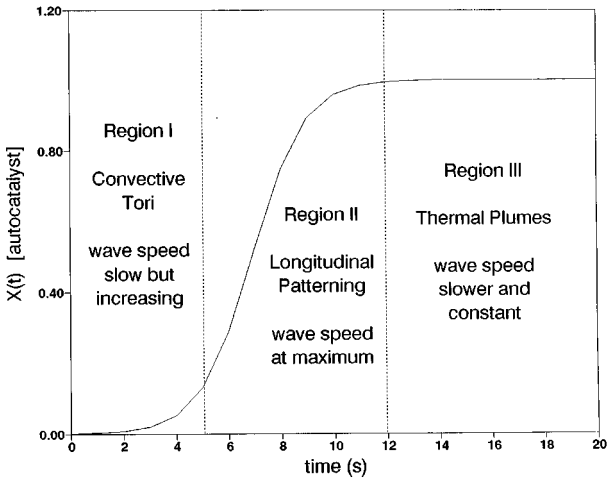

FIG. 3. Plot of Eq. (4) showing the regions with respect to reaction progress. The concentration of the autocatalyst is built up in region I, and thus the wave moves slowly and produces convective tori. After the inflection point, there is a rapid increase in rate as the autocatalyst builds up, giving the longitudinal patterns. The extent of the reaction increases from left to right, but, with a moving boundary, it ceases to change in region III.

patterning appears. Our primary focus in this paper is the mechanism of formation of the concentric patterns in region I (see Fig. 3).

DISCUSSION

Wave speed variations: It has already been established that wave velocity is proportional to the temperature jump at the wave front ΔT [13]. ΔT is proportional to the heat produced by the reaction Q, while Q is a function of the extent of reaction ξ,

$$Q = f(\Delta H_R, \xi, c_{i0}), \tag{1}$$

where ΔH_R is the enthalpy of the reaction, and c_{i0} represents the initial concentrations of the reagents (when a 2:1 stoichiometric ratio of chlorite to thiourea is maintained). Thus for a single reaction and with constant initial concentrations, the variable which controls the amount of heat generated and hence ΔT is ξ. For a bistable and/or excitable reaction system such as the one under study, the extent of reaction ξ is a nonlinear function of the instantaneous chemical reactant concentrations and time. The reaction rate is controlled by the production of autocatalyst HOCl. The rate of production of the autocatalyst is the rate-determining step in all reactions with positive chemical feedback.

$$X + Y \xrightarrow{k} 2X, \quad X = \mathrm{HOCl}, \tag{B}$$

where at $t = 0 [X] = X_0$ and $[Y] = Y_0$. The rate of the reaction is

$$-d[Y]/dt = k[X][Y]. \tag{2}$$

By introducing a progress variable $z = Y(t)$, then

$$X(t) = X_0 + Y_0 - z, \tag{3}$$

A simple integration gives

$$X(t) = \{X_0 + Y_0\}/\{1 + (Y_0/X_0)\exp[-k(X_0 + Y_0)t]\}. \tag{4}$$

A time plot of Eq. (4) which shows the variation of the concentration of the autocatalyst X, with respect to time is sigmoidal [15], and is shown in Fig. 3, in which

$$X(t) = X_0 + Y_0 \quad \text{as} \quad t \to \infty. \tag{5}$$

The plot was plotted with hypothetical concentrations of $[X]_0 = 0.001$ M and $[Y]_0 = 1.00$ M, and a rate constant k of 1.00. The same sigmoidal shape is obtained for any set of initial parameters. Since X is the autocatalyst, we expect a rapid increase in reaction rate with time. The increase in reaction rate increases the instantaneous heat available, Q, and subsequently increases the value of ΔT. At the reaction's maximum rate, the diffusion of reactants into the reaction zone controls the reaction and hence suppresses any possible thermal runaway. This explains the observed rapid acceleration of wave velocity after initiation.

Figure 3 has been labeled, denoting the activity in each region of time. In region I, the wave travels slowly up to the inflection point, where it begins to increase its velocity due to the availability of the autocatalyst HOCl. The convective tori are formed in this region. In region II the reaction rate (and hence production of heat) increases so rapidly that longitudinal patterns are obtained instead of convective tori. Some equilibrium rate of formation of the autocatalyst is attained in region III, and thermal plumes are obtained indefinitely until the wave reaches the end of the vessel. Local diffusion of reactants becomes a factor in region III, and thus diffusion becomes the important factor in determining rate in this region. The moving boundary (wave front), makes Eq. (4) applicable (strictly) only in region I. This simple model also assumes that there is no heat exchange via mass transfer.

Lateral wave velocity is only affected by the Marangoni effect with negligible or no contribution from reaction-diffusion forces, and hence surface velocity V_s [7]:

$$V_s \propto \Delta\sigma/\Delta x, \tag{6}$$

where σ is the surface tension and x is the horizontal spatial displacement coordinate. Thus we expect the top, open surface of the reaction solution to be rapidly moving in the direction of wave propagation, with an equally rapid flow backwards at the bottom of the reaction solution for mass and material balance. This was documented in an earlier publication [12]. The back flow is mostly responsible for the annihilation of the convective tori.

Mechanism of torus formation: The formation of a complete convective roll involves alternately rising and falling regions of reaction solution. Any motion in the vertical z axis has to result from Rayleigh-Bénard (thermogravitational) type of convection [16]. The final convective roll is a result of the coupling between Rayleigh-Bénard (in the form of multicomponent convection) and Marangoni instabilities.

Thermocapillary forces can be estimated from the Marangoni number Ma [17]

$$\mathrm{Ma} = -(\partial\sigma/\partial T)\Delta T l/\eta\chi \tag{7}$$

where l is the length of the free surface, η the dynamic viscosity, and χ the thermal diffusivity. In a particular reac-

tion solution of interest, the only variable is ΔT. The gravitational buoyancy forces can be deduced from the Grashof number Gr [18]:

$$\mathrm{Gr} = -(\partial\rho/\partial T) g \Delta T d^3/\eta\nu \tag{8}$$

where ρ is the solution density, g is Earth's gravity, d is the depth of the solution, and ν is the kinematic viscosity. The values of $\partial\sigma/\partial T$ and $\partial\rho/\partial T$ will determine the relative responses of each force (Marangoni or Rayleigh-Bénard effects) to ΔT. In the chlorite-thiourea reaction we calculated $\partial\sigma/\partial T$ to be $-8.6\times10^{-5}\ \mathrm{N\,m^{-1}\,K^{-1}}$ and $\partial\rho/\partial T$ to be $-0.4\ \mathrm{kg\,m^{-3}\,K^{-1}}$ [6]. In our experiments the Marangoni effect is more sensitive to ΔT than the thermogravitational effect. For example, for $\Delta T = 1\ ^\circ\mathrm{C}$ Ma = 66 600, Gr = 170 for $d = 3.3$ mm and $l = 100$ mm. Thus as the temperature jump ΔT goes up in such shallow solution layers as used in our experiments, we expect a dominance of the thermocapillary effects over buoyancy effects, especially in laterally unbound layers.

Initially, before the reaction gathers speed (through the autocatalytic excitability) both thermocapillary and buoyancy forces are comparable and couple effectively. This is the region in which convective tori are formed. As the reaction's rate increases, thermocapillary forces start to dominate, and vertical buoyancy forces can no longer be effective to display any organization on this time scale. This is the region in which precipitation patterns show longitudinal patterning in the direction of wave propagation. As the wave slows down, the buoyancy forces start to become effective once again, resulting in the volcanic-type thermal plumes behind the wave front which have been previously reported [12].

The series of reactions being studied are known to produce double-diffusive convection and fingering patterns [13,19]. The reaction products (inorganic salts) are heavier than the reactants (uncharged organic molecules) at isothermal conditions [13]. The formation of a convective torus involves the leading edge of the wave front (a) ''fingering'' down the reactant solution, (b) flowing backwards, and then, (c) flowing upwards to complete the cycle (roll). All processes [(a), (b), and (c)] have been observed in this and comparable chemical systems. The only requirement for the convective torus to be formed is chronological coherence of (a)→(b)→(c). Figure 4(a) shows how this can easily be achieved. Process (a) is basic fingering: the product solution is only lighter than the reactant solution when it is at the elevated temperature, $T_0 + \Delta T$. Loss of heat by the front will render the product solution heavier, and this will force it downwards into the reactant solution. At the bottom of the reaction solution is the resident back flow which will sweep the finger backwards, thus effecting process (b). The upward motion of the plume is fueled by the acceleration of the autocatalytic reaction (which leads to a higher ΔT, and hence greater buoyancy) and the availability of reactants. Figure 4(b) shows the experimentally observed temperature profile of a nearly fully formed convective roll which is about 2 mm wide. Although there is a sharp rise in temperature at the wave front, close examination shows an area of chemical reactivity in which the very front tip of the wave does not give the full $\Delta T \approx 3\ ^\circ\mathrm{C}$ temperature jump. This is important in the generation of the fingering regime. At $\Delta T < 3\ ^\circ\mathrm{C}$, the product solution is heavier than the reactant solution, thus establishing the fingering patterns. Further reaction and subsequent attainment of the full temperature jump then renders the product solution lighter.

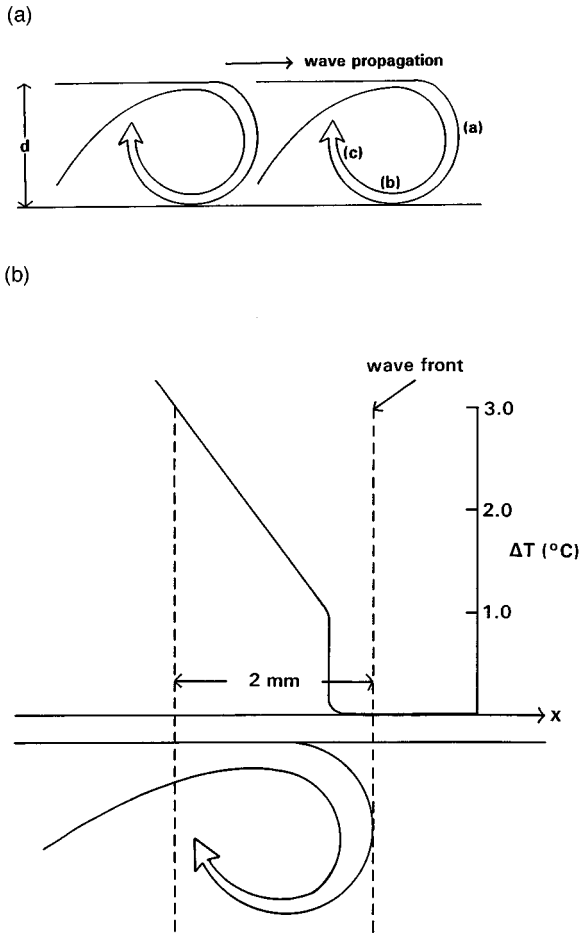

FIG. 4. (a) Schematic diagram of the formation of a series of convective tori. The regions (a), (b), and (c) described in the text are clearly marked. (b) Temperature profile of one of the convective rolls shown in (a). The very front tip of the wave is at a lower temperature than in the bulk of the reacted solution, and hence the ability to form fingering patterns.

Using standard video-imaging data, we observed that the fluid surrounding convective tori spins in the same direction: the top part spins in the direction of wave propagation, but in between tori there is quiescence. Figure 5 shows a schematic sketch of two adjacent convective rolls in which a finger and a plume exist side by side. This explains the transport of $BaSO_4$ crystals from the region. Standard treatment and understanding of convective rolls suggests that a finger and a plume cannot exist side by side, as shown in Fig. 5. This applies only to stationary solutions like the Rayleigh-Bénard convection. In this chemical system, the convective roll on the left is formed first, while the solution now occupied by the roll on the right still contains only the reactant solution. The torus on the right is formed after the one on the left is fully formed. Continuous forward propagation [e.g., region (a) in Fig. 4 moves both forward and downwards] will destroy the circular symmetry of the torus, giving a more oval

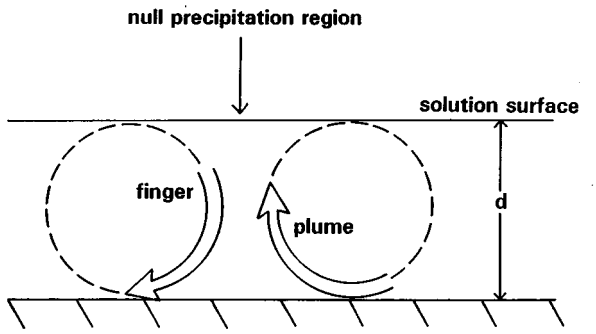

FIG. 5. Diagram showing how two adjacent tori contain fluid moving in opposite directions although they are both spinning clockwise.

shape which gives rise to thermal plumes later in the wave's propagation.

CONCLUSION

The formation of a convective torus is a special case in which the interaction between reaction kinetics, reaction energetics, the Marangoni effect, and thermogravitational effects produces remarkable and coherent yet transient self-organization. The discovery of this type of patterning justifies the conjecture that there exist several other possible mechanisms for stationary pattern formation and general symmetry-breaking bifurcations apart from the standard reaction-diffusion mechanisms. Convective tori have been observed before in pure hydrodynamics systems with lateral heating [20]. Theoretical studies on the Bénard-Marangoni instability with internal heat generation have predicted results such as those reported in this paper [21,22]. The novelty of what we report here is the internal heat generation leading to chemically-driven convective instabilities.

ACKNOWLEDGMENTS

We acknowledge helpful discussions with Dr. Marcus Hauser. We thank the University of Natal for granting leave of absence to one of us (B.S.M.). We also acknowledge the University of Queensland for releasing one of us (T.H.) for sabbatical leave. This work was supported by NSF Grant No. CHE-9632592 awarded to R.H.S.

[1] A. M. Turing, Philos. Trans. R. Soc. London Ser. B **37**, 37 (1952).
[2] M. C. Cross and P. C. Hohenberg, Rev. Mod. Phys. **65**, 851 (1993).
[3] G. Nicolis and I. Prigogine, in *Self-Organization in Nonequilibrium Chemical Systems* (Wiley, New York, 1977).
[4] Q. Ouyang, J. Boissonade, J. C. Roux, and P. De Kepper, Phys. Lett. **134**, 282 (1989).
[5] D. A. Vasquez, J. W. Wilder, and B. F. Edwards, Phys. Fluids A **4**, 2410 (1992).
[6] M. J. B. Hauser and R. H. Simoyi, Chem. Phys. Lett. **227**, 593 (1994).
[7] B. S. Martincigh and R. H. Simoyi, Phys. Rev. E **52**, 1606 (1995).
[8] I. R. Epstein, K. Kustin, and R. H. Simoyi, J. Phys. Chem. **96**, 5852 (1992).
[9] C. R. Chinake and R. H. Simoyi, J. Phys. Chem. **97**, 11 569 (1993).
[10] H. Taube and H. Dodgen, J. Am. Chem. Soc. **71**, 3330 (1949).
[11] G. Rabai and M. Orban, J. Phys. Chem. **97**, 5935 (1993).
[12] B. S. Martincigh, M. J. B. Hauser, and R. H. Simoyi, Phys. Rev. E **52**, 6146 (1995).
[13] C. R. Chinake and R. H. Simoyi, J. Phys. Chem. **98**, 4012 (1994).
[14] A. Belmonte, A. Tilgner, and A. Libchaber, Phys. Rev. E **51**, 5681 (1995).
[15] C. Capellos and B. H. J. Bielski, in *Kinetic Systems* (Wiley, New York, 1972).
[16] Lord Rayleigh, Philos. Mag. **32**, 529 (1916).
[17] M.-J. Char and K.-T. Chiang, J. Phys. D **27**, 748 (1994).
[18] M. K. Smith and S. H. Davis, J. Fluid Mech. **132**, 145 (1983).
[19] J. S. Turner, Annu. Rev. Fluid Mech. **17**, 11 (1985).
[20] D. Villers and J. K. Platten, J. Fluid Mech. **234**, 487 (1992).
[21] H.Q. Yang, Int. J. Heat Mass Transfer **35**, 2413 (1992).
[22] D. Krmpotic, G. B. Mindlin, and C. Perez-Garcia, Phys. Rev. E **54**, 3609 (1996).